Journal of Advanced Concrete Technology
Materials, Structures and Environment

Predicting the Creep Strain of PVA-ECC at High Stress Levels based on the Evolution of Plasticity and Damage

Benny Suryanto, Koichi Maekawa, Kohei Nagai
Journal of Advanced Concrete Technology, volume 11 (2013), pp. 35-48

Scientific paper

Predicting the Creep Strain of PVA-ECC at High Stress Levels based on the Evolution of Plasticity and Damage

Benny Suryanto[1], Koichi Maekawa[2] and Kohei Nagai[3]

Received 10 September 2012, accepted 14 January 2013 doi:10.3151/jact.11.35

Abstract

This paper describes a method for estimating creep deformations of PVA-ECC under high stress levels from short-term tests. To obtain necessary data, a series of accelerated bending and compression creep tests under a sequence of increasing loads were carried out. Of particular interest was to study the evolution of plasticity and damage under varying load levels, and thus allow the rate of plasticity and fracturing as functions of evolving strain and fracture to be determined. Based on these behavioral aspects, predictions of creep of ECC at high stress levels were made. It is found that creep rupture in flexure and compression occurs at nearly the same order of lifetime in a logarithm scale, being the rupture at 90% of flexural strength about one order longer than that under compression. The tensile and compressive strains at rupture, when the load level is decreased from 90% to 75% of the short-term strength, are 1.1-1.4 and 1.6-3.5 times the short-term tensile and compression strain capacities, respectively.

1. Introduction

Polyvinyl Alcohol Engineered Cementitious Composite (PVA-ECC) is a fiber reinforced cement-based material that when subjected to tensile loading exhibits ductile, strain-hardening response. Unlike conventional concrete, which strain-softens under tension, ECC strain-hardens and is able to undergo tensile strain in the order of a few percent and to withstand tensile stresses above the composite's first cracking stress. The large tensile capacity is achieved by allowing the formation of multiple fine cracks, with crack width of less than 100 μm (Li 2003). With these exceptional crack control ability and tensile deformability, ECC is attractive for applications where serviceability and durability are of critical importance. Emerging applications include road patch repair (Li and Li 2009), bridge deck-link slabs (Lepech and Li 2009), damage-tolerant coupling beams (Kanda *et al* 2011), and surface repair of bridge viaducts (Inaguma *et al* 2005).

Further to durability and serviceability advantages, the onsite application of ECC may also be driven by extra stiffness that the material can provide and hence brings structural advantages as well. A good example is in the situation where ECC is intended for strengthening of deteriorated reinforced concrete members such as to enlarge the sides and bottom of a reinforced concrete beam or to increase the thickness of a reinforced concrete member e.g. tunnel linings. In parts that are subjected to tension, the ECC may crack and the tensile stress level that develops in the ECC can be relatively high and hence time-dependent (the ECC cracking stress is typically 0.7-0.9 times the tensile strength). To take full advantage of its strain-hardening property, it is important to study its time-dependent behavior beyond cracking in depth. For instance, the time-dependent creep, if significant, may render the stiffening benefit just briefly described, but it can still be beneficial for other cases such as bonded overlays in terms of relieving shrinkage-induced stresses.

Relatively little research has been, however, undertaken on the time-dependent behavior of ECC, and even a much smaller number on characterizing this behavior under high stress levels. Boshoff and van Zijl (2006, 2007) and Boshoff *et al* (2009) were the first to carry out tensile creep tests of uncracked and cracked specimens. They revealed that time-dependent deformations of cracked ECC occur mainly due to shrinkage of the matrix, delayed cracking, and widening cracks due to fiber pull-out. They also found that the contribution of fiber creep to the overall creep strain of the composite is negligible. Due to the limited number of test specimens, however, no predictive models were proposed. Rouse and Billington (2007) studied the compressive creep strain of ECC at an applied load of about 40% of the compressive strength of the material at 28 days. They demonstrated that the ECC they tested, which contained 6.4 mm long and 8 μm diameter ultra-high molecular weight Polyethylene fibers, exhibited greater creep strain than a similar mixture without fiber. They also indicated that existing predictive models for concrete are suitable for estimating the creep strain at the stress range they investigated. Results of a few tensile and bending tests are available in the appendix of JSCE Recommendation (JSCE 2007), but limited to low to moderate stress levels.

[1]Lecturer, Heriot-Watt University, Institute for Infrastructure and Environment, Edinburgh, Scotland, UK. *E-mail*: b.suryanto@hw.ac.uk
[2]Professor, The University of Tokyo, Tokyo, Japan.
[3]Associate Professor, The University of Tokyo, Tokyo, Japan.

In this paper, an investigation into the creep behavior of ECC under high stress levels is made. A series of accelerated short-term creep tests were performed instead of conventional creep tests, which take a long time to perform and are tedious as such tests typically require a large number of specimens to be tested under different load levels. Also, short-term test was preferable as the rate of creep is generally logarithmic in nature. The accelerated test proposed involved the testing of a series of single specimen under a sequence of constant load levels. The main intention was to relate the evolving damage and plasticity accumulated in the ECC, from the individual load sequence, to the evolution of elastic and plastic strains. On the basis of these observations, the creep behaviors of ECC under variable and constant load levels are discussed in both tension and compression.

The rest of this paper is structured as follows: Section 2 describes the theoretical background, Section 3 describes the experimental program, Section 4 presents the short-term behavior of ECC under variable load levels and includes empirical formulations for describing this behavior, and Section 5 provides the prediction of the short- and long-term behaviors of ECC under sustained loads.

2. Evolution of plasticity and fracture in cracked PVA-ECC

2.1 Background

The evolution of plasticity and fracture is postulated to be the two main factors that govern the extent of time-dependent strain in ECC under high stress levels. To study this behavioral aspect, consider the schematic representation of the stress-strain curve for ECC in tension as shown in **Fig. 1**. First, let us assume that the material is loaded up to a certain stress level beyond cracking, and then the load is held constant. Under this constant loading, it can be expected that plasticity and fracture in the ECC will grow with time and correspondingly the creep strain. Ideally, this is a continuous process, but let us visualize this as a series of discrete steps. From this individual step, unload and reload the specimen, before and right after this individual step, to obtain the state of the material. This enables us to determine the creep evolution in the ECC with time.

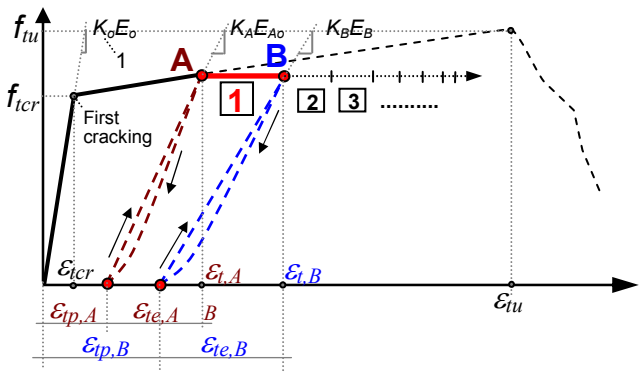

Fig. 1 Conceptual illustration of the proposed approach.

Based on the above-mentioned concept, let consider the strain states occurring between Points A and B, which are the beginning and end of the first loading cycle over a time interval Δt. By assuming a linearization of plastic strain evolution, the average rate of plastic strain during this time interval can be approximated as:

$$\frac{d\varepsilon_{tp,1}}{dt} = \frac{\varepsilon_{tp,B} - \varepsilon_{tp,A}}{\Delta t} \tag{1}$$

where $\varepsilon_{tp,A}$ and $\varepsilon_{tp,B}$ are the tensile plastic strains at Points A and B, and can be obtained from rapid stress release from the two states. The average tensile plastic strain during the time interval Δt can be approximated as:

$$\varepsilon_{tp,1} = \frac{\varepsilon_{tp,A} + \varepsilon_{tp,B}}{2} \tag{2}$$

As the elastic strain also changes with time, the average elastic strain can also be approximated as:

$$\varepsilon_{te,1} = \frac{\varepsilon_{te,A} + \varepsilon_{te,B}}{2} \tag{3}$$

During the same time interval, the evolving damage can be calculated in a similar manner to above in terms of the average rate of fracture and the average fracture as given by:

$$\frac{dK_{t,1}}{dt} = \frac{K_{t,A} - K_{t,B}}{\Delta t} \tag{4}$$

$$K_{t,1} = \frac{K_{t,A} + K_{t,B}}{2} \tag{5}$$

where K_t is the stiffness at a time of interest (i.e. Point A) relative to uncracked stiffness, K_o.

Once the fracture $K_{t,1}$ and the elastic strain $\varepsilon_{te,1}$ are determined, they can be related to the stress field $f_{t,1}$ in the following manner:

$$f_{t,1} = K_{t,1}\varepsilon_{et,1} \tag{6}$$

where $\varepsilon_{te,1} = \varepsilon_{tt,1} - \varepsilon_{tp,1}$, and $\varepsilon_{tt,1}$ is the average tensile strain during the State 1.

2.2 Basic modeling strategy

Two components of deformations are considered to make up the total time-dependent strain under high stress levels: the plastic strain component and the elastic strain component. The first component is considered to represent the permanent deformation incurred during loading that is directly related to the plasticity evolution, while the second component is used to characterize the instantaneous reversible strain and is associated with the

space-averaging elastic response of the material. In this paper, the increase in elastic strain with time is linked to progressive fracturing.

To determine the change in plasticity, this study uses the data from the strain field as the state of stress is not readily available. El-Khasif and Maekawa (2003) demonstrated the feasibility of this concept for conventional concrete in compression and it is of interest to explore its applicability for a different material such as ECC. The plasticity rate is considered to be a function of the plastic strain ε_p that is accumulated in the ECC, to account for loading history, and the elastic strain ε_e, to account for damage progress and the applied stress level, as:

$$\frac{d\varepsilon_p}{dt} = f\left(\varepsilon_e, \varepsilon_p\right) \tag{7}$$

Two parameters are also proposed to determine the fracturing rate dK/dt: the average elastic strain ε_e and fracture parameter K as given by:

$$\frac{dK}{dt} = f\left(\varepsilon_e, K\right) \tag{8}$$

where K is the ratio of the current stiffness to the initial stiffness. In this equation, the elastic strain ε_e is also considered as an indicator of the applied stress level, while the fracture parameter K is used to account for the influence of loading history (El-Khasif and Maekawa 2003). These two equations are to be determined in the later part of this paper using the method proposed in the previous section.

3. Experimental programs

3.1 Test setup

A series of short-term creep experiments were carried out to check the validity of the proposed modeling. The experimental program involved the testing of fourteen small-scale beams in flexure and six cylinders in compression. Each of the specimens was tested at a sequence of increasing load levels. A detailed description of the experimental program is given below.

The beams were all prismatic, of rectangular section, 50 mm deep and 100 mm wide. They were all simply supported over a span of 500 mm and tested under four-point bending. The center span between the two point loads was 110 mm. Beams B1 to B3 and B11, taken as the control specimens, were loaded to failure under monotonically increasing displacement at a rate of 0.8 mm/min. Other beams (Beams B4 to B9, B12, and B14) were subjected to cyclic loads under variable load levels. The following loading protocol was adopted:

L1. The beam was first loaded to a predefined load level in a displacement-controlled mode at a rate of 0.8 mm/min.
L2. Once the intended load level was achieved, loading was then altered from displacement control to load control, allowing the load to be held constant for an intended time span (i.e., 10 minutes).
L3. Loading was then switched back to displacement control in order to unload and then reload the beam to the same or a higher load level in a more accurate manner. This unloading and reloading process took approximately one to two minutes.
L4. Loading procedures L2 and L3 were repeated several times until the beam failed (either due to loading or creep rupture when the load was held constant).

The only exception to the Loading Procedure L2 was when testing Beams B9 and B14 in which the displacement instead of the load was held constant (noted by R in **Table 1**).

Table 1 summarizes the maximum load attained for each loading cycle in percentage of the ultimate load capacity of the control beams and the corresponding time duration in seconds. It was decided to have diverse time steps and load levels such that the consistency of the proposed method could be well verified. For Beams B4 to B8, the initial load level was in the range of 66% to 82% of the average static strength. The load level was kept constant for a period of time (i.e. 275 seconds; see Beam B4 at a load level of 69%), and was subsequently raised in steps when the increase in the flexural tensile strain was no longer significant. The test duration was kept in the range of about 3 to 20 minutes to provide a reasonable compromise between accuracy due to the linearization process and number of cycles that may induce additional damage. The load level for Beams B12 and B13 was set at moderate levels in order to investigate the behavior under this load level as well. When the increase in the flexural tensile strain was no longer significant the load level was subsequently increased (same as the previous series), or the time duration was lengthened.

For a comparison, six additional 100×200 mm PVA-ECC cylinders were tested to investigate the time-dependent nonlinearity in compression under high stress levels. Cylinders C1 and C2 were tested under static displacement-controlled loads to obtain the compressive strength, while the other four cylinders were subjected to cyclic displacements using the same procedure as for the beams.

3.2 Instrumentation

Figure 2(a) shows the instrumentation used in the flexural tests that includes load cell to record the applied load, two LVDTs to measure average mid-span deflection, and two cable transducers to measure surface tensile strains. The cable transducers were glued on the bottom surface of each beam over the constant moment span [see **Fig. 2(c)**]. The cylinders were instrumented with a compressometer having two LVDTs to record the average compressive strain, and a load cell to record the applied load [see **Fig. 2(b)**].

Table 1 Test specimens and a summary of applied loading.

ID	Objective	Load pattern % of capacity (time in seconds)	ID	Objective	Load pattern % of capacity (time in seconds)
B1-B3 B11	Static capacity	100% (710, on average)	C1-C2	Static capacity	100% (365, on average)
B10	Cyclic response	71%, 77%, 84%, 86%, 90% 95%, 98%, 98%, 90%	C3	To determine the time-dependent properties of PVA-ECC	60% (298, 300, 300) 70% (300, 304, 300) 80% (298, 300, 298) 90% (88, 86, 86), 90%
B4	To determine the time-dependent properties of PVA-ECC	69% (275), 71%(369,606,602,422) 81% (302, 606, 619, 609, 606, 612, 604, 605), 90% (106)	C4		75% (598, 596) 85% (602, 598), 89%
B5		68% (306, 318, 302) 77% (303, 298, 303) 82% (302, 339), 87% (302,306) 93% (185, 101-CR)	C5		60% (56), 65% (56) 70% (58), 75% (56) 80% (58), 85% (56) 90% (34), 100%
B6		66% (264,244,326,601, 648,601) 82% (305-CR)	C6		75% (300, R) 90% (298, R), 100%
B7		70% (1204, 1202, 1205) 79% (185, 1206, 1204, 1207) 88% (308, 305), 93% (63, 44-CR)	Notes: - CR: Creep rupture. - R: Displacement was held constant. - The load in percentage is the load level normalized by the average static strength obtained from the control specimens. - Numbers in the brackets are time in seconds, representing the time span when the specimen was subjected to a constant load.		
B8		82% (183, 605, 1261) 85% (1804, 1806), 100%			
B9		72% (616,R), 84% (623,R), 100% (605,R),104% (631,R),108%			
B12		59% (606, 1220, 2412) 65% (324, 1706), 95%			
B13		55% (602, 1210, 2406, 2528) 70% (612, 1212, 1808, 2352), 95%			
B14		58% (332, 604, 604) (all R) 73% (306, 604, 602, 600) 84% (304, 602, 600), 100%			

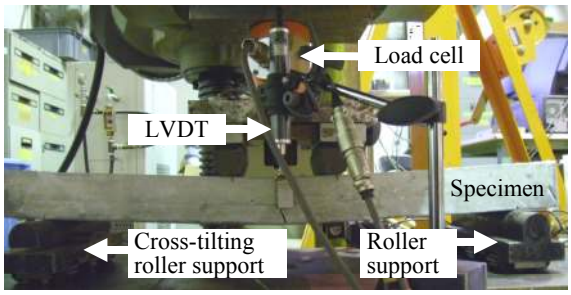

(a) Beam specimen during testing

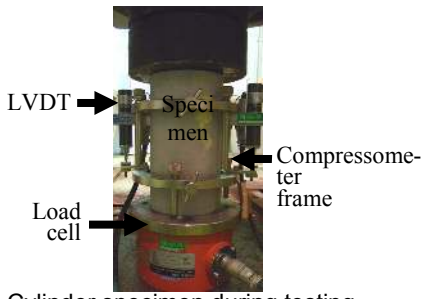

(b) Cylinder specimen during testing

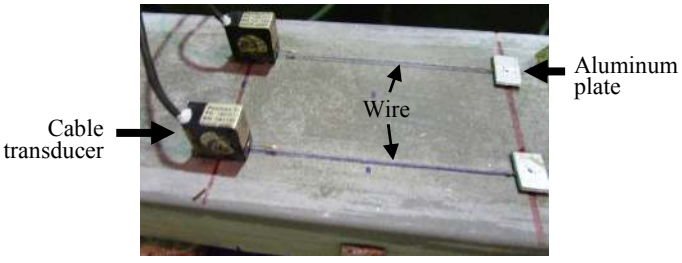

(c) Two cable transducers glued on the bottom surface of a beam

Fig. 2 Test setup and instrumentation.

3.3 Material and fabrication

A premixed PolyVinyl Alcohol (PVA)-ECC material available in the Japanese market was used in this study. The amount of materials for one batch of 32 liters, which includes the amounts of the premix products, water, chemical admixtures (Polycarboxylic-acid based SP, expansive and shrinkage reducing agents, and AE agent), and the mixing procedure can be found in the Appendix of JSCE Recommendation (JSCE 2007, pp. 129-135). A summary of the main mixture proportion is

Table 2 Mix proportion for PVA-ECC (JSCE 2008).

W/(C+FA) (%)	Water (kg/m^3)	S/(C+FA) (%)	PVA Fibers (%), in vol.
42.2	350	70	2.0

Note: W is water, C is ordinary Portland cement, FA is fly ash, and S is fine sand.
PVA fibers: diameter is 0.04 mm, length is 12 mm, and tensile strength is 1,600 MPa.

given in **Table 2**.

The mixing procedure was done by first inserting all the dry components, water, and chemical admixtures into a twin shaft concrete mixer. They were then thoroughly mixed for 10 minutes. Immediately after this, the workability and air content of the fresh ECC were checked. The average slump flow of the fresh ECC measured from the standard slump flow test was about 600 mm, while the average air content was about 11%.

After confirming these fresh mixture properties, the fresh ECC was poured into the middle of each steel mold at once and shredded laterally. The slurry was also poured into plastic cylinder molds vertically in three layers. All the specimens were then covered with plastic sheets. After a day of curing period, they were all stripped off and then cured in a water tank in a room with a temperature of 18±3°C until the testing date of 28 to 34 days of age.

4. Test results and discussions

4.1 Static response

Figure 3 shows the observed responses of control beams and control cylinders subjected to monotonically increasing displacement to failure. As the figure shows, the four beams exhibited a highly ductile behavior. The beams failed in flexure at an average load of 4.68 kN, which was highly above the first cracking load. The average midspan deflection and tensile strain at failure were 8.31 mm and 1.74%, respectively. The control cylinders failed at an average compressive stress of 39 MPa, with the corresponding peak strain of 0.38%. All load and strain values in the rest of this paper will be expressed as a percentage of these values.

4.2 Cyclic response

Figure 4 and **Fig. 5** show the observed load-deflection (or -deformation) and corresponding deformation-time responses of each specimen over the observation period. The loads shown are normalized by the ultimate load capacity of the control beams. These data are presented in this section to give a general indication of the responses of the material under cyclic and short-term sustained loads.

The test results shown in **Fig. 4(a)** and **Fig. 4(b)** indicate that the effects of cyclic and short-term sustained loads on the static capacity and ductility of the beams and the cylinders are minor. Except for Beam B6 that failed prematurely at about 83% of its static capacity, all other beams were able to sustain a maximum load of approximately 90% of their short-term static capacities. No appreciable differences in ductility were evident in all of the beams tested and even a slight increase in ductility was observed in the cylinders. Moreover, the experimental results constantly display significant residual deflections and plastic strains accumulating through each loading cycle. Similar observations were made for specimens subjected to cyclic tension by Jun and Mechtcherine (2010).

From the deformation versus time plots in **Fig. 5(a)** and **Fig. 5(b)**, it can be inferred that the observed tensile and compressive strains under a constant applied load increase with time, implying that the strain is time-dependent. At lower load levels, for instance see the responses of Beams B12 and B13 and Cylinder C3, the increasing rate is seen to drop off quickly with time and hence the strains tend to level off. They start to increase again once the load levels are increased. At higher load levels, the strains are seen to keep increasing over the time period investigated (see Beam B7 and Cylinder C4, for instance).

Furthermore, it is interesting to note that although the observed strains under a constant compression stress

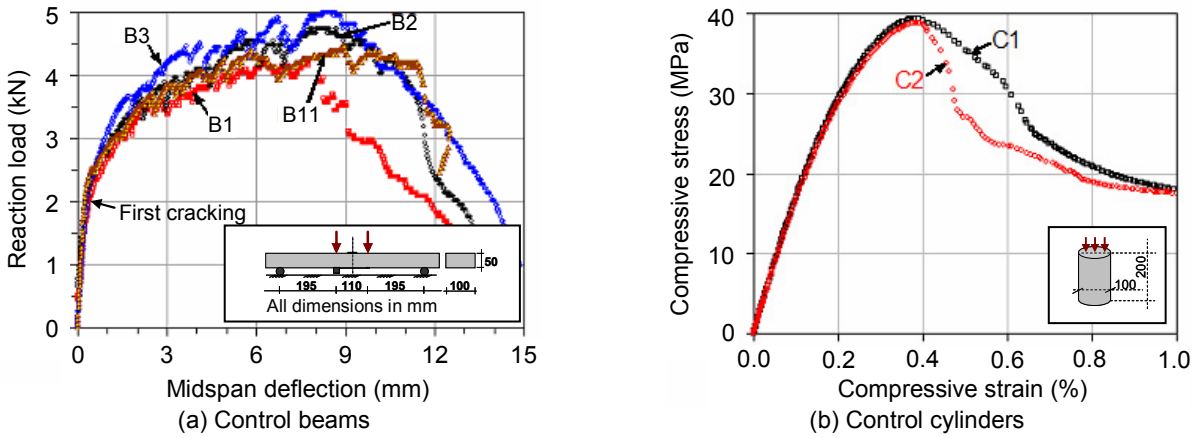

(a) Control beams (b) Control cylinders

Fig. 3 Test specimens under static loads.

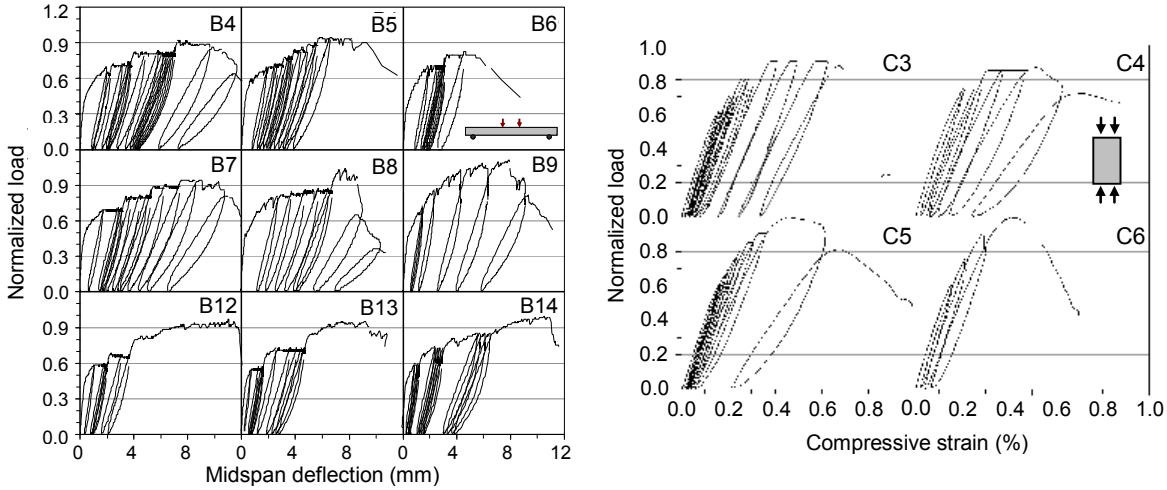

(a) Responses under 4-point bending (b) Responses under compression

Fig. 4 Macroscopic responses under cyclic loads.

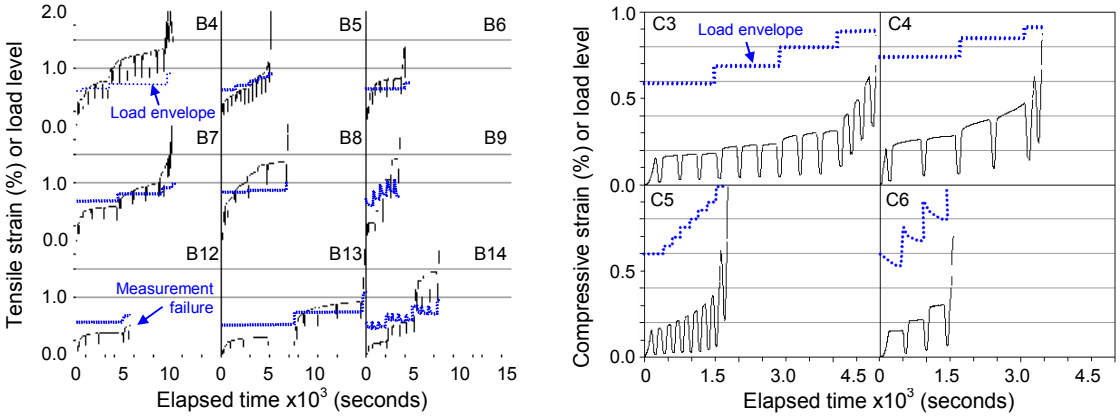

(a) Time-strain responses under 4-point bending (b) Time-strain responses under compression

Fig. 5 Time-strain responses under cyclic loads.

always exhibit a gradual increase, the tensile strains sometimes show a sudden increase possibly due to either the formation of a new crack or the mergence of pre-existing cracks, forming a single through crack throughout the beam width.

With these data at hand, attempts were then made to extract the parameters that are associated with the plasticity (elastic strain ε_e, plastic strain ε_p, and plasticity rate $d\varepsilon_p/dt$) from the time-deformation responses, and the parameters that are related to fracturing (elastic strain ε_e, fracture parameter K, and fracturing rate dK/dt) from the load-deformation responses. The procedures outlined in Section 2 were used and the results are presented in the following section.

4.3 The evolution of plasticity and damage

To establish a clear relation of the parameters representing the states of plasticity and fracturing, all the data obtained from the cyclic tests are plotted on the same figure in **Figures 6(a)-(d)** according to the types of loading. **Figure 6(a)** and **Fig. 6(b)** show the observed plastic strain rate versus the normalized plastic strain from the results of bending and compression tests, respectively, while **Fig. 6(c)** and **Fig. 6(d)** shows the corresponding fracturing rate versus the fracture parameter extracted from the test results. The fracturing rates shown are multiplied by 10^4 to make them in the same order of magnitude to the plasticity rate. The markers indicate the experimental data, while the lines indicate best-fit curves that will be discussed in the next subsection. The data corresponding to nearly the same magnitude of elastic strain (± 75-100 micron) were plotted in the figures using the same markers. The numbers on the lines having the same color with the markers indicate the corresponding normalized elastic strains. It is interesting to note that when the data from individual load cycles were clustered according to the magnitude of the elastic strain, these data cluster reasonably well into a trend, particularly those at smaller elastic strain values. The following paragraphs summarize the trend observed.

From the extracted plasticity data shown in **Fig. 6(a)** and **Fig. 6(b)**, there is a notable trend of decreasing plastic rate with increasing plastic strain for the same elastic strain value. Since the increasing rate in plastic strain under a constant load is generally higher than that in elastic strain, plasticity under sustained load can thus

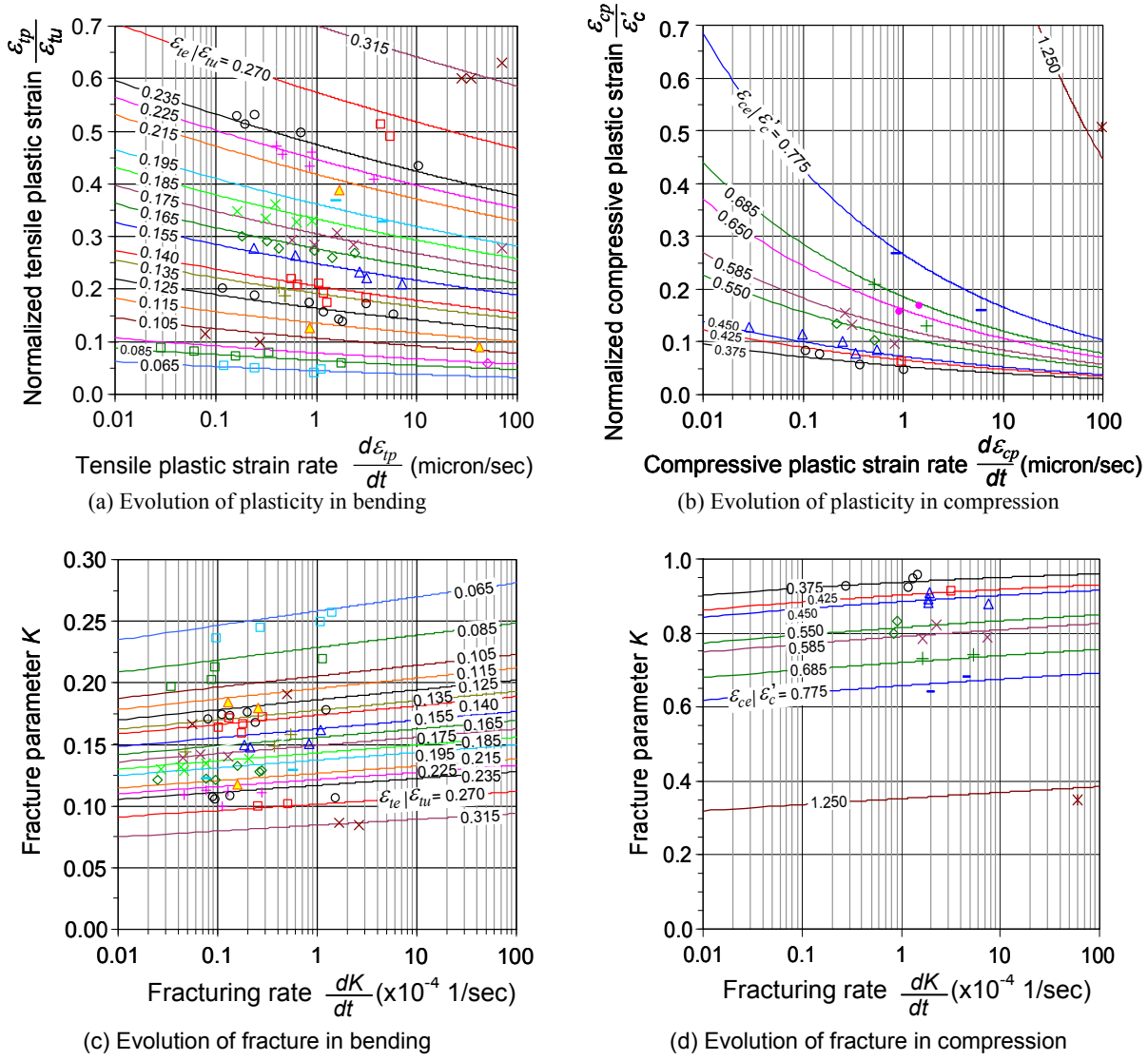

(a) Evolution of plasticity in bending

(b) Evolution of plasticity in compression

(c) Evolution of fracture in bending

(d) Evolution of fracture in compression

Fig. 6 Extracted plasticity and fracture.

be expected to proceed at a decreasing rate. It is also apparent from the figures that the curves related to large elastic strains have steeper gradients. As the elastic strain can be considered an indicator of the load level applied, it can be inferred that the rate of plasticity should decrease more slowly with increasing load level. This explains the quick dropping off of strain rate with time at the early stages of loading of Beams B12 and B13, when subjected to lower load levels [see **Fig. 5(a)**]. Finally, it is also evident from the two figures that a greater part of the short-term strain in bending is highly irrecoverable, while a greater part of the short-term strain in compression is highly recoverable. At high stress levels, for instance, the normalized tensile plastic strains are 0.5 to 0.6 of the static tensile strain capacity, while the plastic compressive strains are only about 0.2 to 0.3 of the static compressive strain capacity.

From the fracturing data shown in **Fig. 6(c)** and **Fig. 6(d)**, it appears that the fracturing rate decreases with increasing damage (decreasing fracture parameter K) when the elastic strain is held constant. It can also be seen from the two figures that the data having nearly the same magnitude of elastic strain form curves with a somewhat similar gradient, implying that load level has a minor influence on the fracturing rate. The only exceptions are the flexural responses at lower stress levels represented by the curves corresponding to normalized elastic strains of 0.065 and 0.085 that show a notably steeper slope, possibly due to more intense formation of multiple cracking at this stress range. Finally, as also apparent from the two figures, the fracture parameters K in flexure appear to be lower than about 0.25, over the range of the load investigated, while those under compression are in the range of 0.6 to 0.9. The small values of K in flexure over the range of stresses studied indicate that the ECC underwent sudden change of stiffness soon after experiencing state changes from uncracked to cracked.

4.3 Empirical formulations

In this section, empirical relations that were chosen to fit with test data shown in **Fig. 6(a)** and **Fig. 6(b)** are presented. In accordance with Equation 7, the following empirical equation is proposed to provide a measure of the plasticity rate:

$$\frac{d\varepsilon_p}{dt} = \left(\frac{a}{\varepsilon_p / \varepsilon_u} \right)^{1/b} \tag{9}$$

where a and b are two parameters that depend on the magnitude of elastic strain. In this equation, the parameter a is used as an indicator of the extent of plastic strain ε_p that has been accumulated in the ECC [this is associated with the position of the curve along the vertical axis of **Fig. 7(a)**], while the parameter b is used to control the degree of plastic strain increment [this is related to the slope of the curves in **Fig. 7(a)**]. The following equations are proposed to express the two:

$$a = \begin{cases} 2.83\dfrac{\varepsilon_{te}}{\varepsilon_{tu}} - 0.19\,;\, a > 0.045 & \textit{for flexural tension} \\ 0.012\exp\left(4\dfrac{\varepsilon_{ce}}{\varepsilon_{cu}}\right) & \textit{for compression} \end{cases} \tag{10}$$

$$a = \begin{cases} -0.13\dfrac{\varepsilon_{te}}{\varepsilon_{tu}} + 0.08 & \textit{for flexural tension} \\ 0.2\dfrac{\varepsilon_{ce}}{\varepsilon_{cu}} + 0. & \textit{for compression} \end{cases} \tag{11}$$

Note that, for tension, ε_{te} is normalized with ε_{tu}, while for compression ε_{ce} is normalized with the strain corresponding to compressive strength ε_{cu}).

To provide an estimate of the fracturing rate dK/dt, the following expression is proposed in accordance with Equation 8:

$$\frac{dK}{dt} = \frac{1}{10^4}\left(\frac{p}{K-1}\right)^{\frac{1}{q}} \tag{12}$$

where p is a damage indicator that controls the degree of fracturing K and q is a power term that controls the degree of fracturing increment, with p and q being a function of the normalized average elastic strain. The p parameter determines how the curve moves vertically in **Fig. 7(c)** and **Fig. 7(d)**, while the q parameter controls the slope of the curves. These two parameters were calibrated against the test data, and the following expressions are proposed:

$$p = \begin{cases} -0.11\ln\left(\dfrac{\varepsilon_{te}}{\varepsilon_{tu}}\right) - 1.0425 & \textit{for flexural tension} \\ -0.7\dfrac{\varepsilon_{ce}}{\varepsilon_{cu}} + 0.2\,;\; p > -0.98 & \textit{for compression} \end{cases} \tag{13}$$

$$q = \begin{cases} 0.001\left(\dfrac{\varepsilon_{te}}{\varepsilon_{tu}}\right)^{-0.7} & \textit{for flexural tension} \\ 0.012\left(\dfrac{\varepsilon_{ce}}{\varepsilon_{cu}}\right)^{-2.1} + 0.005 & \textit{for compression} \end{cases} \tag{14}$$

It should be noted that all the parameters obtained above are suitable for PVA-ECC with the mixture proportion listed previously in **Table 2** and shall be calibrated for a different ECC, as more information becomes available. The parameters for flexure might be sensitive to the amount and type of fiber used (particularly if the fibers do not form chemical bond and form only frictional bond with the ECC matrix), while the parameters for compression might be less sensitive to this issue. Future research in this area is needed.

5. Predictions of the time-dependent creep under high stress levels

Having obtained the empirical equations (Equations 9 to 14) and **Fig. 6**, one can thus use either one to estimate the time-dependent creep of ECC. A flowchart describing the step-by-step calculation procedure is given in **Fig. 7**. For a given stress level, one should firstly obtain the values of immediate strain and fracture, and then assume a time increment Δt. Since creep is logarithmic in nature, it is best to start with a very small time increment (e.g. 1 second), especially if there is a rapid change in plasticity or fracturing such as after the load is held constant or increased to a new level. As time progresses, the time increment can be increased, if necessary. One can then use **Fig. 6(a)** to **Fig. 6(d)**, if the use of chart is preferable, start at the vertical axis of the figures, move horizontally to the graph line, and then across to the horizontal axis to get the plasticity/fracturing rate, or otherwise, directly use Equations 9 and 12. Afterward, Equations 16 to 18 can be used to update the values of the strains and fracture, and thus the total strain at the current time step (Equation 19). This process can be repeated as necessary or until failure occurs. In the calculation, creep rupture is distinguished by a rapid increase in total strain as the rate of elastic strain becomes infinitely large, while the rate of plastic strain remains comparatively small. In general, this whole calculation process is tedious, if performed, by hand, but is relatively straightforward with an Excel spreadsheet. The following sections present results obtained from the predictions.

5.1 Short-term creep under variable load levels

This section presents results obtained for the prediction of the test beams subjected to variable load levels. In order to simplify the prediction, the following assumptions were made to take into account the changes in the load level:

1. The increase in creep strain at intermediate stress levels during unloading and reloading process is

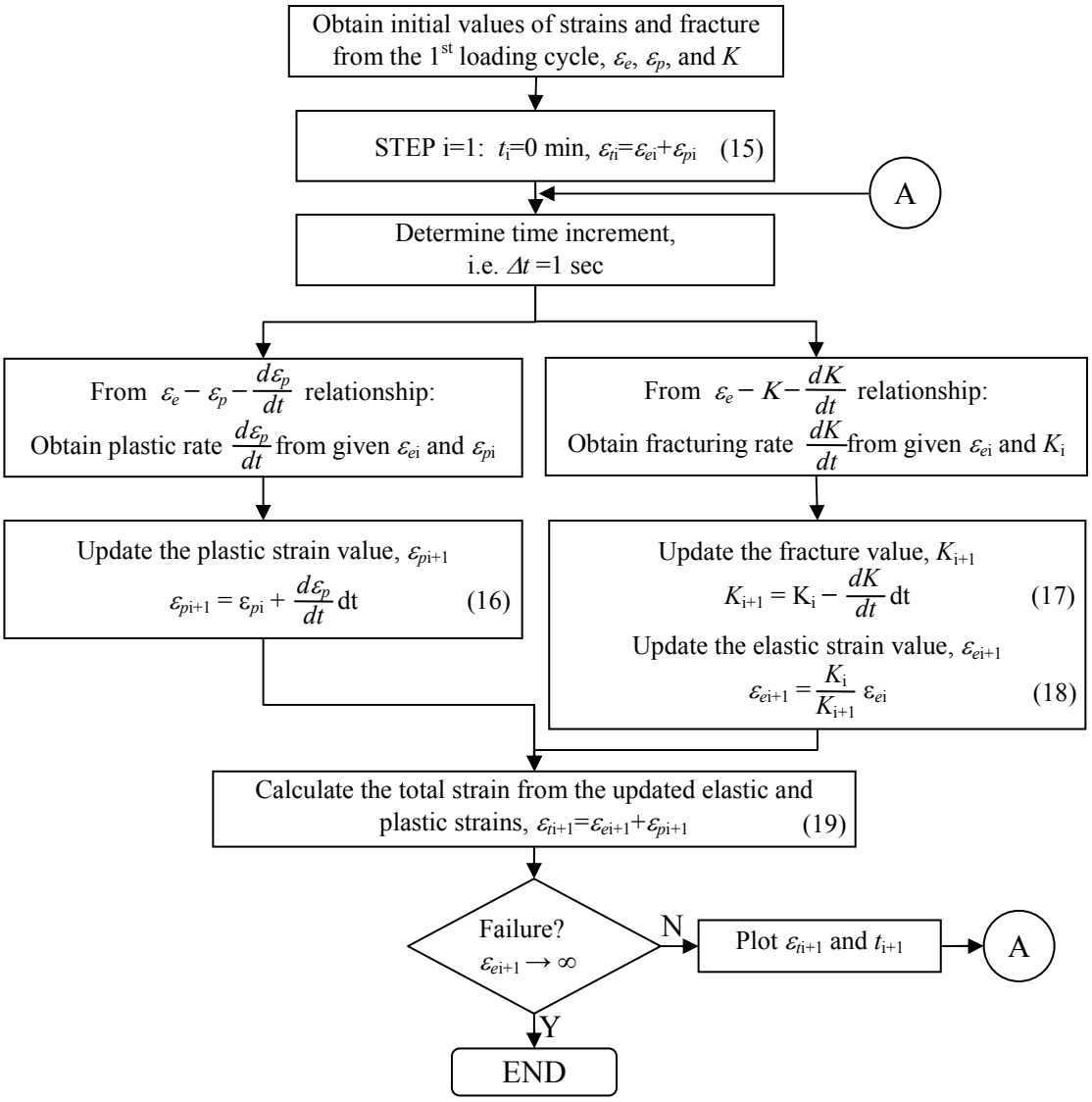

Fig. 7 Procedure for computing time-dependent strains under sustained load.

negligible.

2. The increase in load level is proportional to the elastic strain as given by:

$$\varepsilon_{ej+1} = \frac{P_{j+1}}{P_j}\varepsilon_{ej} \quad (20)$$

where, P_{j+1} and P_j indicate the current and previous load levels, and ε_{ej+1} and ε_{ej} are the corresponding strains, respectively. The strain ε_{ei+1} obtained from Equation 18 can be used as input for ε_{ej}.

3. The increase in plasticity and fracturing when the load is increased occurs at once while the load change is taking place. To take into account this effect, the second part of Equations 17 and 18 is replaced with a lump sum additional plastic strain or fracture. These values were approximated from the load cycles before and right after the increase in load.

Figure 8 compares the predicted and observed response of selected test beams. Note that the unloading and reloading response from the observed response was ignored and hence the observed responses plotted in the figure are the compressed version of that shown previously in **Fig. 5(a)**. In general, there is a reasonable agreement between the generated creep strains and the experimentally observed strains. The following two paragraphs summarize the comparison.

For Beam B4, the agreement of the two is reasonable. The predicted strain over this first loading stage replicates the observed strain well. The predicted strain over the second load stage was, however, smaller than the observed strain. The agreement over the next load stages appears to be reasonable, although the analysis slightly overestimates the strain rate during the later parts of the third loading stage. The analysis successfully predicts the creep failure soon after the load is increased to about 90% of its static capacity. For Beam B5, the agreement

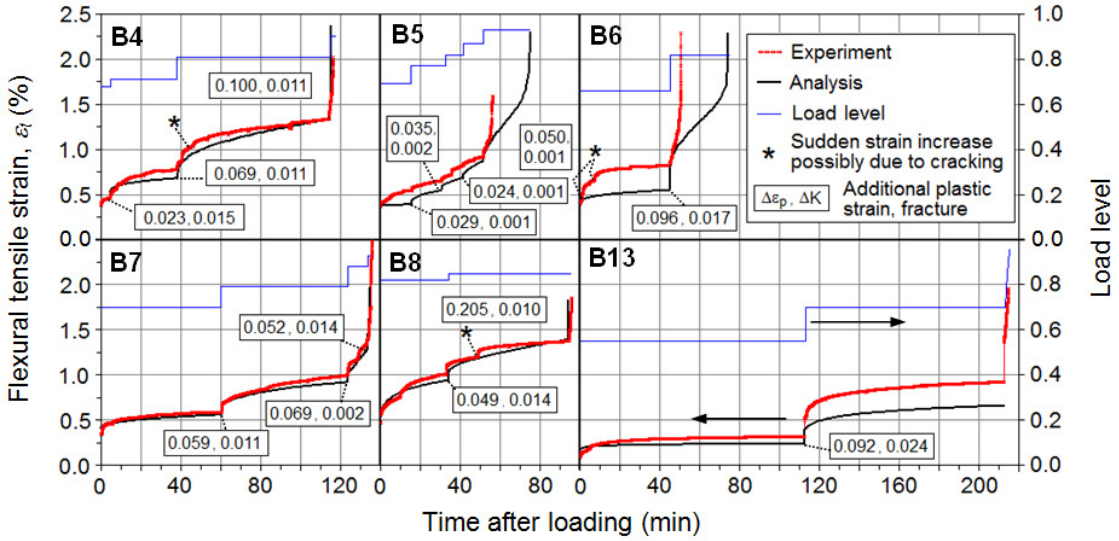

Fig. 8 Comparison of predicted and observed short-term responses of selected beams.

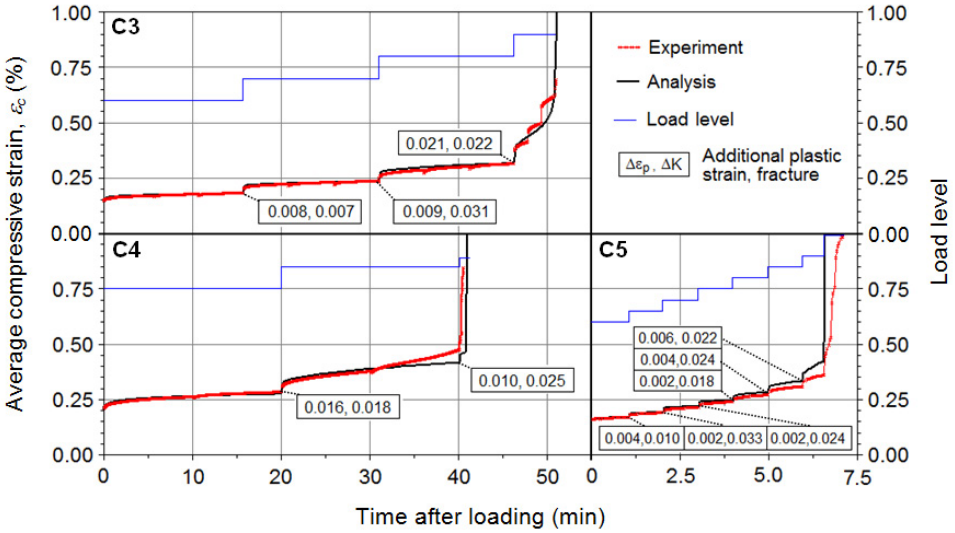

Fig. 9 Comparison of predicted and observed short-term responses of selected cylinders.

of the two is also reasonably good. Although the analysis tends to underestimate the observed strain rate over the first loading stage, it replicates the general pattern of the observed response over the remainder load stages well. The lifetime was somewhat overestimated by about 15 minutes possibly as a result of neglecting the loading and reloading process (note that this specimen was subjected to more cycles, but shorter in time, and hence time taken during the cyclic process was relatively more significant). For Beam B6, the agreement of the two is worse. A significant underestimation of strain at early to intermediate stages and a significant overestimation of the time to failure can be observed. Unlike the observed strain that increases rapidly after loading possibly due to either the development of a new crack or the mergence of existing cracks, the predicted strain appears to increase more gradually. It is likely that if the extensive cracking did not happen, this beam would be able to sustain the increased load longer, as found analytically.

For Beam B7, there is an excellent agreement between the predicted and observed strains. The predicted response appears to follow the trend of the observed response very well. An excellent agreement can also be seen between the predicted and observed responses of Beam B8, given that this specimen was subjected to high load levels from the very beginning. From the comparison of predicted and observed response of Beam B13, it appears that the predicted strain underestimated the observed strain over the two loading periods applied. This warrants further investigations into the time-dependent behavior under low to intermediate load levels.

Figure 9 compares the predicted and observed response of selected test cylinders. Similar to the previous figure, it should be noted that the observed creep strains plotted in the figure are the compressed version of those shown in **Fig. 5(b)**. As can be seen from the figure, the

agreement between the predicted and observed compressive strains is excellent. When compared to the results presented earlier, it appears that the creep behavior in compression is much more stable than that in flexure, allowing the compressive creep behavior to be predicted more satisfactorily.

5.2 Short- to long-term creep under constant load levels

In order to illustrate the usefulness of the above method, an example of the prediction of the creep of hypothetical ECC at high stress levels was made. Four different load levels were considered: 75%, 80%, 85%, and 90% of the static strength. Data that were not available were estimated by plotting the available data in **Fig. 10** and then making best fit lines. As can be seen, the magnitude of strain and fracture shows a linear trend to applied load level, except for the tensile fracture that indicates a quadratic trend. **Table 3** summarizes the values of initial strains and fracture used.

Figure 11(a) and **Fig. 11(b)** show the computed normalized total strains versus time. The computed strains are normalized to static strain capacity to give a clear picture of their relative values. In general, it appears that the development of the creep strain and the lifetime are clearly very much dependent on the applied load level. The higher the load being sustained, the earlier the time

Table 3 Input variables for prediction.

Load level	Tension				Compression			
	ID	$\varepsilon_{te}/\varepsilon_{tu}$	$\varepsilon_{tp}/\varepsilon_{tu}$	K_t	ID	$\varepsilon_{ce}/\varepsilon_{cu}$	$\varepsilon_{cp}/\varepsilon_{cu}$	K_c
75%	P9	0.080	0.082	0.264	C4	0.494	0.052	0.894
80%	P8	0.117	0.154	0.189	-	0.542*	0.082*	0.864*
85%	-	0.160*	0.220*	0.149*	-	0.590*	0.112*	0.834*
90%	P10	0.200	0.288	0.127*	C6	0.639	0.142	0.803

Note: * approximated values.

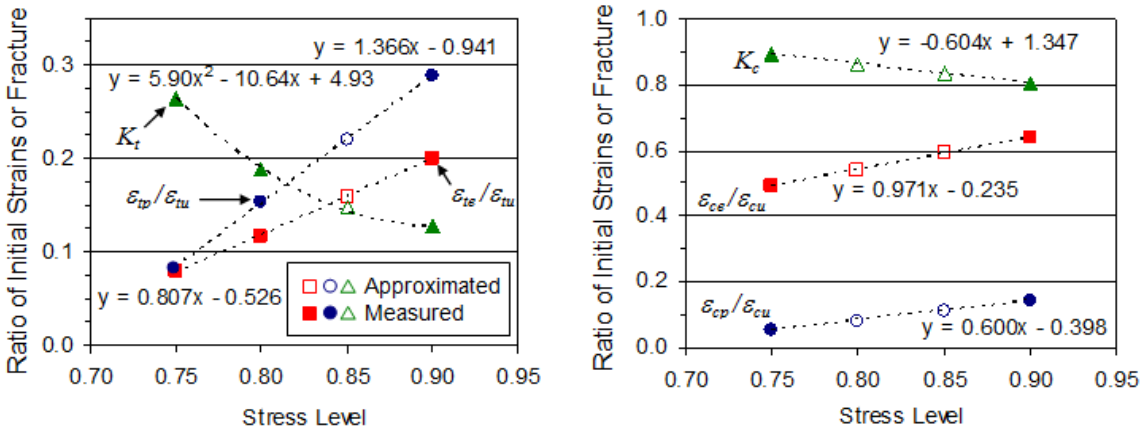

(a) Flexure (b) Compression

Fig. 10 Measured and approximated values of initial strain and fracture parameter.

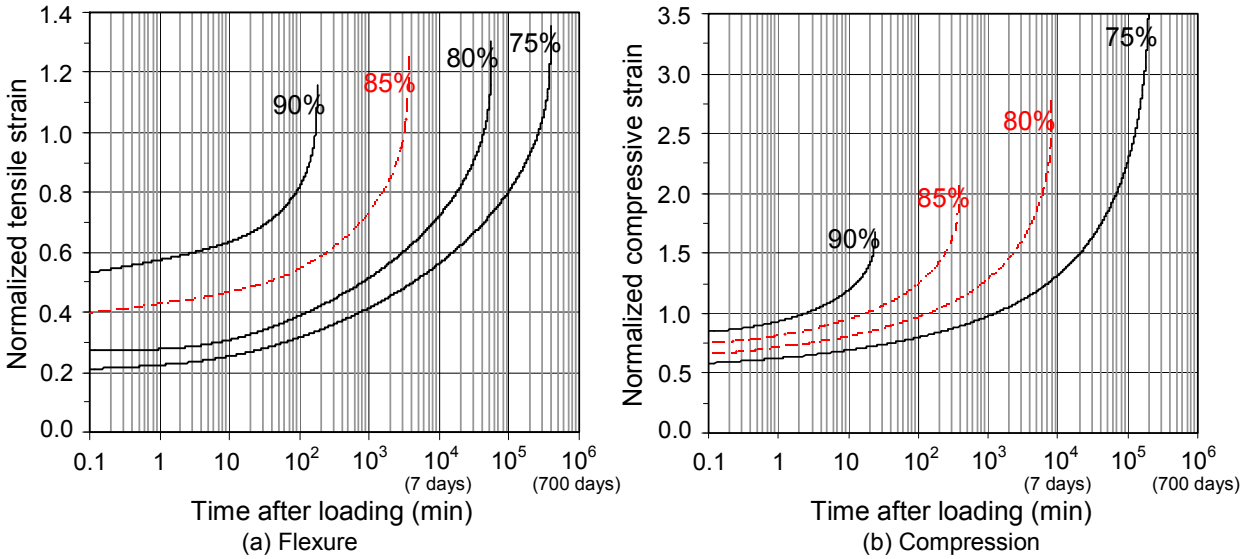

(a) Flexure (b) Compression

Fig. 11 Predicted deformations under sustained loads for various initial stresses, for hypothetical ECC beams with 2% of PVA fibers.

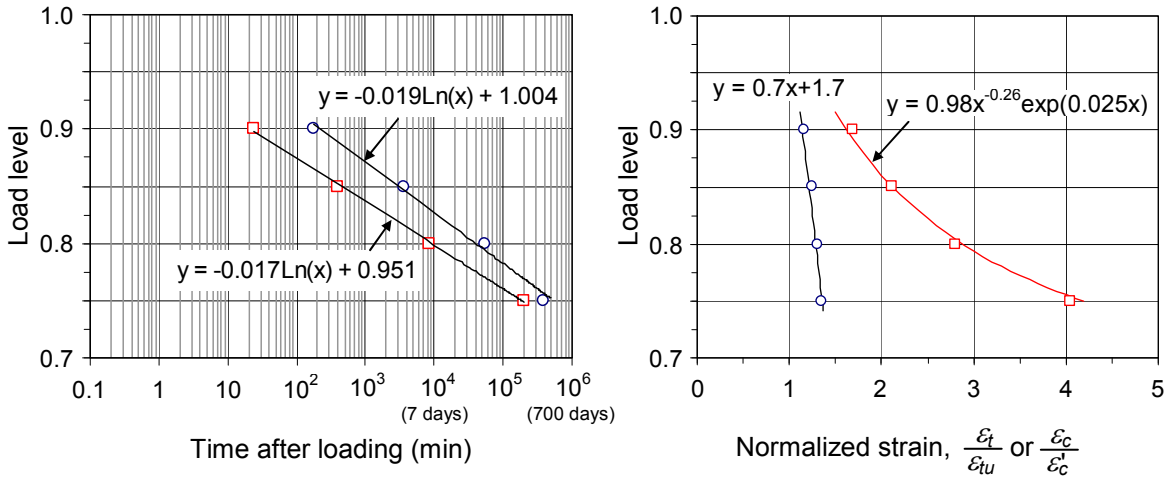

(a) Time to rupture (b) Strain at rupture

Fig. 12 The influence of load sustained at upon time to rupture and strain at rupture, for hypothetical ECC beams with 2% of PVA fibers.

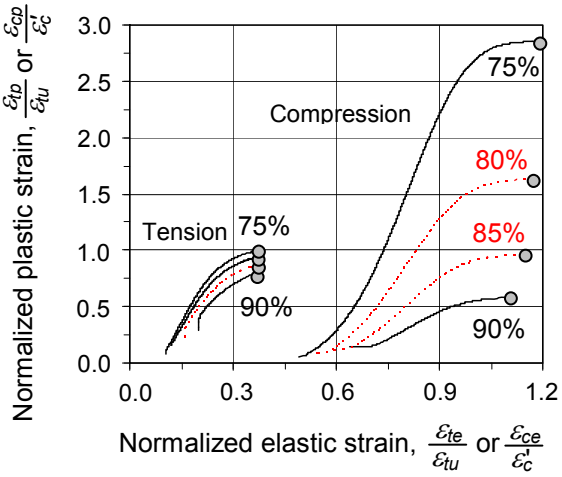

Fig. 13 Predicted elastic and plastic ECC strain components, for hypothetical ECC beams with 2% of PVA fibers.

to failure and the smaller the strain at failure is. Over the range of load levels investigated, the strain at rupture is seen to be always larger than the short-term strain capacity, indicating the ability of the material to maintain its large strain capacity when subjected to sustained load.

Figure 12 summarizes the dependence of the time to rupture and the corresponding strain on the load level applied. Regardless of the loading condition, it is predicted that the time to rupture will increase with decreasing load level. As can be seen in **Fig. 12(a)**, a somewhat linear trend between the magnitude of load and logarithm of time to rupture is apparent. It is unclear, however, whether this linear trend would remain at lower stress levels. Interestingly, time to failure under flexural loading is seen to be almost at the same order to that under compression, being at 90% of the static strength of approximately an order of magnitude longer than that under compression and being that the difference between the two diminishes as the load level is decreased. Similar to the time to rupture, it is predicted that the strain at rupture will also increase with decreasing load level [see **Fig. 12(b)**]. The load level is seen to be a far more significant factor affecting the creep strain capacity under compression than that under flexure. It is predicted that as the load level is decreased, the tensile strain capacity in flexure will increase almost linearly, while the compressive strain capacity will increase somewhat exponentially. In the load range of 75 to 90% of the static strength, it is predicted that the compressive strain capacity will be about 1.6 to 3.5 of the static strain capacity, while the tensile strain capacity will be in the range of 1.1 to 1.4 times of the static strain capacity.

To explain the notable differences in the magnitude of strain at rupture under the two loading conditions, the normalized elastic strain versus normalized elastic strain plot depicted in **Fig. 13** is discussed. It is evident from this figure that the load level, for the range investigated, has a great influence on the magnitude of plastic compressive strain, a minor influence on that of plastic tensile strain, and a negligible influence on that of both elastic compressive and tensile strains. As the stress is decreased from 90% to 75% of the short-term compressive strength, the magnitude of plastic compressive strain is predicted to increase from approximately 0.6 to almost 3 times of the short-term compressive strain capacity. It is thus obvious that it is this large plastic strain that had contributed to the large compressive creep strain at lower load levels observed previously in **Fig. 12** and **Fig. 13**. Regarding the effects on the plastic tensile strain, it is predicted that the magnitude of the tensile strain will only increase from about 0.8 to 1.0 times of the static tensile strain capacity under the same load range. This narrow strain range indicates that only a moderate change in average crack width would happen. Further tests need to be carried out to confirm this phenomenon. Finally, the minor influence of the load level on the magnitude of the elastic strain can be seen from the marginal range of the normalized elastic tensile and plastic strains of approximately 0.36 and 1.1-1.2 of the

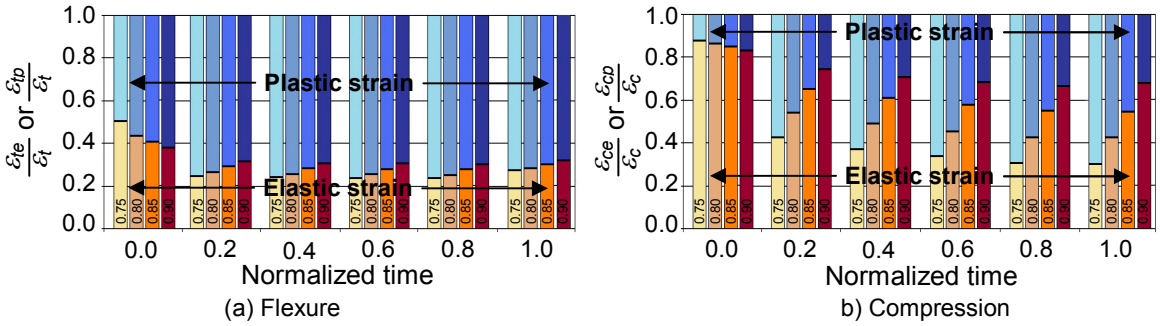

Fig. 14 Predicted plastic and elastic strain components under 75% to 90% of static capacity.

static strain capacity, respectively.

Finally, it is of interest here to obtain the significance of plasticity and fracturing on the creep deformation after loading. **Figure 14** shows the dependence of the proportion of plastic and elastic strain components on discrete time points after loading normalized by the time at rupture. As can be seen from **Fig. 14(a)**, it is predicted that the evolution of plasticity is the predominant factor of tensile creep at early time, as illustrated by the nearly constant proportion of elastic and plastic strains for normalized lifetime greater than 0.2. Plasticity is also predicted to be the greater part of the total creep deformation. The influence of the stress level appears to be insignificant. By contrast, it is predicted that the compressive stress level affects the proportion of the two strain components quite significantly [see **Fig. 14(b)**]. The contribution of the plastic strain to the total strain is predicted to increase as the stress level is decreased, particularly if the stress levels are lower than 80% of short-term strength. At these stress levels, it is also apparent that the plasticity evolution progesses during the early lifetime, as marked by the nearly constant proportion of the two strain components for the normalized lifetime greater than 0.2.

6. Concluding remarks

An investigation into the creep behavior of PVA-ECC under sustained loads is presented. The investigation started with the attempt to trace the changes in elastic strain, plastic strain, and fracture in the ECC from a series of specimens that were tested under a sequence of increasing load levels. This enabled the determination of the rate of plasticity as a function of the strains accumulated in the ECC, as well as, the rate of fracturing as a function the existing damage and the magnitude of elastic strain. On the basis of this concept, predictions of the time dependence under variable and constant stress levels were made. The following conclusions can be drawn:

Short-term creep tests under increasing load levels

(1) External load if applied below 90% of the static strength for few tenths of minutes was found not to significantly affect the strength and ductility of the ECC specimens.

(2) Significant portions of short-term strains of ECC under compression are recoverable, while those of tensile strains under flexural loading are irrecoverable.

The evolution of plasticity and fracturing

(3) When the elastic strain is held constant, plastic rate appears to decrease as the plastic strain increases. The plastic strain evolution is more significant at higher stress levels.

(4) When the elastic strain is kept constant, it appears that fracturing rate decreases as the extent of damage increases. Stress level is seen to have a minor effect on fracturing rate.

ECC specimens under varying loads

(5) The reasonable agreement between the predicted and observed response of a series of ECC specimens tested under different load sequences and load durations indicates the viability of the proposed method to characterize the short-term behavior of ECC subjected to sustained loads.

(6) It appears that the model proposed for flexural tensile creep performs better at higher stress levels. The correlation between the predicted and observed flexural tensile strains is reasonably good. A better correlation is seen from the predicted and observed responses in compression. Based on the work presented, future works will be directed toward formulating a more general model for uniaxial tension.

Hypothetical ECC specimens under constant loads

(7) Creep rupture is predicted to occur under load levels of 75% to 90% of the static strength. The logarithm of time to rupture is shown to be inversely proportional to the load level. Time to rupture under compression at 90% load level appears to be approximately one order of lifetime shorter than that under flexure. This difference appears to diminish with decreasing load level.

(8) Load level appears to affect creep strain under compression more significantly than that under flexure. As the load level is decreased from 90% to

75% of the static strength, the tensile and compressive strains at rupture are 1.1 to 1.4 times and 1.6 to 3.5 times the tensile strain and compressive strain capacities, respectively.

(9) Plastic tensile strain is seen to account for a greater part of the total strain. The same circumstance is observed in compression when the applied stress levels are lower than about 80% of the short-term strength.

References

Boshoff, W. P. and van Zijl, G. P. A. G., (2006). "Time-dependent response of ECC: Characterisation and modelling of creep and creep Fracture." *In*: G. Fischer and V. C. Li, Eds. *International RILEM Workshop on HPFRCC in Structural Applications*, Honolulu 23-26 May 2005. USA: RILEM Publications, PRO 49, 125-134.

Boshoff, W. P. and van Zijl, G. P. A. G., (2007). "Time-dependent response of ECC: Characterisation of creep and rate dependence." *Cement and concrete research*, 37(5), 725-34.

Boshoff, W. P., Mechtcherine, V. and van Zijl, G. P. A. G., (2009). "Characterising the time-dependant behaviour on the single fibre level of SHCC: Part 1: Mechanism of fibre pull-out creep." *Cement and Concrete Research*, 39(9), 779-786.

El-Khasif, K. F. and Maekawa, K., (2004). "Time-dependent nonlinearity of compression softening in concrete." *Journal of Advanced Concrete Technology*, 2(2), 233-247.

Inaguma, H., Seki, M., Suda, K. and Rokugo, K., (2006). "Experimental study on crack-bridging ability of ECC for repair under train loading." *In:* G. Fischer and V. C. Li, Eds. *International RILEM Workshop on HPFRCC in Structural Applications*, Honolulu 23-26 May 2005. USA: RILEM Publications, PRO 49, 499-508.

JSCE (2007). "Recommendations for Design and Construction of High Performance Fiber Reinforced Cement Composite with Multiple Fine Cracks (HPFRCC)." *Concrete Library*, 127. (in Japanese)

JSCE (2008). "Recommendations for Design and Construction of High Performance Fiber Reinforced Cement Composite with Multiple Fine Cracks (HPFRCC) with Multiple Fine Cracks." *Concrete Engineering Series*, 82.

Jun, P. and Mechtcherine, P., (2010). "Behaviour of Strain-hardening Cement-based Composites (SHCC) under monotonic and cyclic tensile loading, Part 1 - Experimental investigations." *Cement & Concrete Composites*, 32, 801-809.

Kanda, T., Nagai, S., Maruta, M. and Yamamoto, Y., (2011). "New high-rise R/C structure using ECC coupling beams." *In:* R. D. Toledo Filho, F. A. Silva, E. A. B. Koenders, and E. M. R. Fairbairn, Eds. *2nd International RILEM Conference on Strain Hardening Cementitious Composites*, Rio de Janeiro, 12-14 December 2011. France: RILEM Publications S. A. R. L, 289-296.

Lepech, M. D. and Li, V. C., (2009). "Application of ECC for bridge deck link slabs." *Materials and Structures*, 42(9), 1185-1195.

Li, V. C., (2003). "On engineered cementitious composites (ECC) - A review of the material and its applications." *Journal of Advanced Concrete Technology*, 1(3), 215-230.

Li, M. and Li, V. C., (2009). "Influence of Material Ductility on Performance of Concrete Repair." *ACI Material Journal*, 106(5), 419-428.

Rouse, J. M. and Billington, S. L., (2007). "Creep and shrinkage of high-performance fiber-reinforced cementitious composites." *ACI Materials Journal*, 104(2), 129-136.